JGR Oceans

RESEARCH ARTICLE
10.1029/2018JC014175

Intraseasonal Variability of Surface Salinity in the Eastern Tropical Pacific Associated With Mesoscale Eddies

Audrey Hasson[1], John Thomas Farrar[2], Jacqueline Boutin[1], Frederick Bingham[3], and Tong Lee[4]

[1]Sorbonne Université CNRS, IRD, MNHN, Laboratoire d'Océanographie et du Climat: Expérimentations et Approches Numériques, LOCEAN, Paris, France, [2]Center for Marine Science, University of North Carolina Wilmington, Wilmington, NC, USA, [3]Department of Physical Oceanography, Woods Hole Oceanographic Institution, Woods Hole, MA, USA, [4]Jet Propulsion Laboratory, California Institute of Technology, Pasadena, CA, USA

Key Points:
- Eddies originating from the Gulfs of Tehuantepec and Papagayo fall into three categories and have a persistent surface salinity signature
- This study confirms the hypothesis that eddies formed in coastal regions can grow in the open ocean
- Satellite sea surface salinity measurements reveal new information on eddy properties

Supporting Information:
- Supporting Information S1
- Figure S1
- Movie S1

Correspondence to:
A. Hasson,
audrey.hasson@locean.upmc.fr

Citation:
Hasson, A., Farrar, J. T., Boutin, J., Bingham, F., & Lee, T. (2019). Intraseasonal variability of surface salinity in the eastern tropical Pacific associated with mesoscale eddies. *Journal of Geophysical Research: Oceans*, *124*, 2861–2875. https://doi.org/10.1029/2018JC014175

Received 15 MAY 2018
Accepted 20 FEB 2019
Accepted article online 28 MAR 2019
Published online 29 APR 2019

Abstract Strong variability in sea surface salinity (SSS) in the Eastern Tropical Pacific (ETPac) on intraseasonal to interannual timescales was studied using data from the Soil Moisture and Ocean Salinity, Soil Moisture Active Passive, and Aquarius satellite missions. A zonal wave number-frequency spectral analysis of SSS reveals a dominant timescale of 50–180 days and spatial scale of 8°–20° of longitude with a distinct seasonal cycle and interannual variability. This intraseasonal SSS signal is detailed in the study of 19 individual ETPac eddies over 2010–2016 identified by their sea level anomalies, propagating westward at a speed of about 17 cm/s. ETPac eddies trap and advect water in their core westward up to 40° of longitude away from the coast. The SSS signatures of these eddies, with an average anomaly of 0.5-pss magnitude difference from ambient values, enable the study of their dynamics and the mixing of their core waters with the surroundings. Three categories of eddies were identified according to the location where they were first tracked: (1) in the Gulf of Tehuantepec, (2) in the Gulf of Papagayo, and (3) in the open ocean near 100°W–12°N. They all traveled westward near 10°N latitude. Category 3 is of particular interest, as eddies seeded in the Gulf of Tehuantepec grew substantially in the vicinity of the Clipperton Fracture Zone rise and in a region where the mean zonal currents have anticyclonic shear. The evolution of the SSS signature associated with the eddies indicates the importance of mixing to their dissipation.

Plain Language Summary Large (150–250 km) and slow-moving (westward 14.5 km/day) eddies formed near the Pacific coasts of Mexico and Costa Rica show anomalies in sea surface salinity. The recent satellite missions (Soil Moisture and Ocean Salinity, Soil Moisture Active Passive, and Aquarius) help us characterize the sea surface salinity signal within the eddies during their entire lifelong journey. We show evidence along the latitude of 10°N that these eddies trap and move waters within their cores with reduced exchanges with outside waters for 1,000 to 2,000 km. Three categories of eddies were established according to the location where they first reach detection threshold. Eddies detected in the open ocean are of particular interest, as they are greatly affected (growing rates, timing, and pathways) by the bathymetry of the Clipperton fracture zone (between 5,000 and 2,000 m deep) even though their only reach a few hundred meters of depth.

1. Introduction

The Eastern Tropical Pacific (ETPac) is a region of complex atmospheric and oceanic circulations. Easterlies and tropical storms are funneled through the topography of the southern North America-Central American Cordillera (Figure 1), creating the so-called gap winds. They are especially strong over the Gulfs of Tehuantepec and Papagayo (Stumpf & Legeckis, 1977). In the ocean, an intricate current system exists east of 120°W, with considerable meridional flow that helps to connect opposing zonal tropical currents to one another. The eastward flowing North Equatorial CounterCurrent (NECC) and Equatorial Undercurrent terminate in the ETPac where the westward flowing North Equatorial Current (NEC) and South Equatorial Current (SEC) originate (see Kessler, 2006, for a review of the ETPac oceanic circulation). Strong interannual, seasonal, and intraseasonal variability in the gap winds and in the Intertropical Convergence Zone (ITCZ) leads to intense variations in the ocean circulation.

The subseasonal variability of the ETPac is characterized by large eddies formed every year from October to July in the Gulfs of Tehuantepec and Papagayo (Willett et al., 2006). Eddies are important features affecting

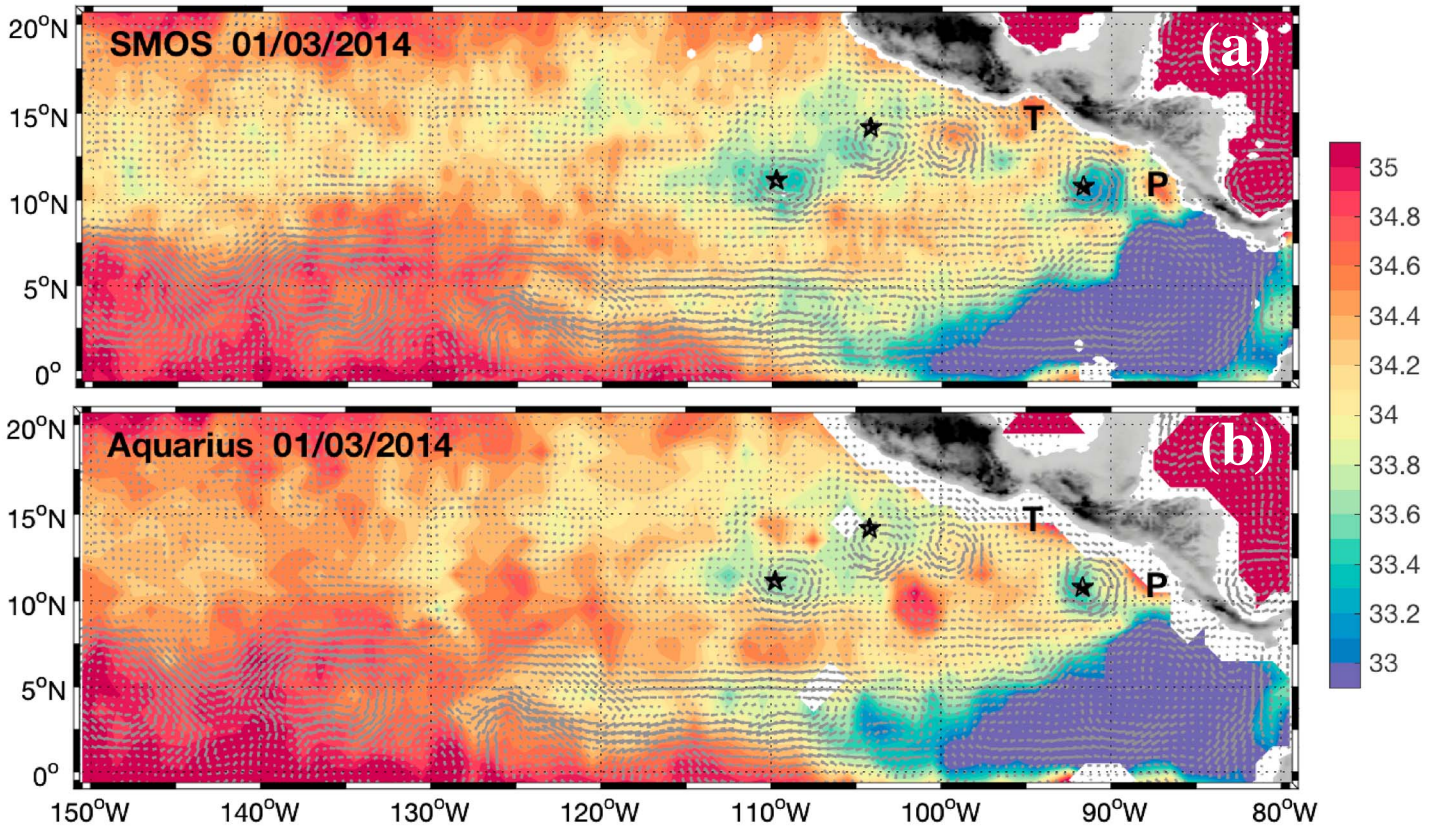

Figure 1. 1 March 2014 SSS from (a) SMOS and (b) Aquarius overlaid with Copernicus Marine and Environment Monitoring Service currents. Selected eddies from the Chelton-Schlax-Sameslon Atlas (Chelton, Gaube, et al., 2011; Chelton, Schlax, & Sameslon, 2011; see section 2.1 for details) are highlighted with a star in the center. Black-shaded areas on land are over 500 m in elevation and highlight the Pan-American topography. The Gulfs of Tehuantepec and Papagayo are denoted by a T and P, respectively. Three eddies are identified from the current structures with apparent associated low SSS.

oceanic dynamics and biology globally, as they transport momentum, heat, salt, and chemical and biological properties (Chelton, Gaube, et al., 2011; Chelton, Schlax, & Sameslon, 2011; Dong et al., 2014; Gonzalez-Silvera et al., 2004; Müller-Karger & Fuentes-Yaco, 2000; Zhang et al., 2014).

These eddies were first observed by Stumpf and Legeckis (1977) and have been the subject of many studies (Adams & Flierl, 2010; Chang et al., 2012; Farrar & Weller, 2006; Giese et al., 1994; Willett et al., 2006). For instance, on 1 March 2014 three of these eddies were present in the ETPac (Figure 1). Palacios and Bograd (2005) estimated an average of 2.2–3.5 eddies per year with a lifetime above 1 month emanating from the Gulfs of Tehuantepec and Papagayo between 1992 and 2004. Up to seven eddies (with lifetimes >1 month) were observed between November 1998 and March 1999 by Gonzalez-Silvera et al. (2004) during a La Niña event. They propagate westward between 9°N and 13°N with a speed of 9 to 19 cm/s and a radius between 50 and 250 km as summarized by Adams and Flierl (2010) from nine studies based on observations of sea surface temperature (SST), ocean color, seal level anomaly (SLA), and dynamic height. Because eddies are quasiperiodic in time and longitude once they are far from the coast, Farrar and Weller (2006) described 10°N eddies as westward-propagating oscillations with a zonal wavelength of 500 to 1,650 km and an estimated phase speed of 11.3 $\pm$ 5.5 cm/s. Ocean color measurements have revealed anticyclonic eddies traveling from the Gulfs of Tehuantepec and Papagayo for up to 4 months until they reach the NECC, highlighting their importance for the transport of organisms and nutrients away from the southern North America and Central American coasts (Gonzalez-Silvera et al., 2004; Müller-Karger & Fuentes-Yaco, 2000; Samuelsen & O'Brien, 2008).

Previous studies have discussed possible generation mechanisms from both low-frequency wind variations that create instabilities of the currents (Périgaud, 1990) and high-frequency winds such as the Tehuantepec and Papagayo jets (Barton et al., 2009; Giese et al., 1994; Müller-Karger & Fuentes-Yaco,

2000). Intense bursts of "Nortes" (or "Tehuanos") winds channeled through the Sierra Madre mountain range generate the so-called gap winds. These wintertime bursts often lead to Tehuantepec jets, which are associated with eddies formed in the Gulf of Tehuantepec. Papagayo jets related to Gulf of Papagayo eddies (PE) can be caused by gap winds but are more often driven by trade wind variations or tropical storms (Chelton et al., 2000). The formation due to the conservation of potential vorticity as the NECC is deflected north into the Costa Rica Coastal Current has also been discussed (Hansen & Maul, 1991). Recent studies based on observations and models have agreed that a combination of these mechanisms is responsible for the largest, farthest-reaching eddies (e.g., Chang et al., 2012; Farrar & Weller, 2006; Liang et al., 2012).

The signature of these long-lived eddies in SLA, ocean color, and SST have been previously discussed in the literature (see Willett et al., 2006, for a review). Their signature in Sea Surface Salinity (SSS) has however not yet been investigated.

The tropical Pacific Ocean displays a large spatial contrast of SSS. The far ETPac is characterized by a low SSS feature known as the ETPac freshpool, which Guimbard et al. (2017) delineated by the 34-isohaline. The ETPac freshpool is shaped to first order by precipitation from the ITCZ, by the seasonal upwelling and by the tropical current system (NEC, NECC, and SEC) driven by low-frequency winds. The ETPac freshpool has a strong seasonal cycle, as it extends from the coast to about 120°W from January to April then spreads westward to reach 170°W by October–November (Guimbard et al., 2017). In this region, air-sea CO_2 fluxes have been shown to be under the competitive influences of rain-induced freshening and ocean dynamics, and satellite observations of SSS and SST provide very useful information to interpret and infer sea surface CO_2 partial pressure (Brown et al., 2015). The seasonal SSS signal created by intense precipitation associated with the ITCZ is then advected poleward by the Ekman transport (Bingham & Lee, 2017; Yu, 2015). Equatorial surface currents were found to be crucial in the seasonal zonal extension of the freshpool (Guimbard et al., 2017). The NECC brings saltier waters in January–April, whereas to its north and south, the NEC and SEC advect fresher waters westward, away from the coastal area. Variability of the low SSS waters closer to the southern North America and Central American coasts is moreover driven by the seasonal cycle of local smaller-scale currents and seasonal upwelling (Alory et al., 2012; Kessler, 2006). The present study examines the intraseasonal SSS variability of the ETPac that has not been adequately studied.

Recent advances in SSS observation from space have enabled new monitoring of the distribution and variability of SSS from the interannual and large scale to the intraseasonal and the large mesoscale. From 2010 to the present, the Soil Moisture and Ocean Salinity (SMOS) mission (Kerr et al., 2010), the Aquarius/SAC-D satellite mission (Lagerloef et al., 2008), and the Soil Moisture Active Passive (SMAP) mission (Piepmeier et al., 2017) have retrieved SSS with unprecedented spatiotemporal coverage. SSS is a key parameter influencing the ocean circulation through its effect on density but is also a tracer of air-sea freshwater fluxes and ocean dynamics. Satellite missions have revealed that SSS anomalies associated with eddies can be monitored for months near river outflows (Fournier, Vandemark, et al., 2017; Fournier, Vialard, et al., 2017) and large anomalies can be seen in the tropical Pacific Ocean following El Niño and La Niña events (Hasson et al., 2014, 2018). Studies have also shown that remotely sensed SSS in the tropical Pacific Ocean be used to trace mesoscale features such as tropical instability waves (Lee et al., 2012; Melnichenko et al., 2017; Yin et al., 2014) and heavy rainfall associated with large convective cells in the ITCZ (Supply et al., 2017).

Eddies generated in the Gulfs of Tehuantepec and Papagayo and traveling westward along 10°N have a distinct SSS signature (Figure 1). This paper examines the intraseasonal SSS variability and associated physical mechanisms in the ETPac in relation to these eddies. The observational data sets and methods are described in section 2. Results are presented in the section 3, including the examination of SSS variability at 10°N in the ETPac (section 3.1), the associated transport (section 3.2), and the eddies' evolution (section 3.3). Discussion and concluding remarks are given in section 4.

2. Data and Methods

2.1. Data Sets

The satellite-derived SSS, SLA, currents, precipitation, and evaporation used in the present study are briefly described in this section.

The European Space Agency Earth Explorer mission SMOS has been retrieving SSS from January 2010 to present (Kerr et al., 2010). SMOS' native spatial resolution is about 50 km, and global coverage is acquired in about 5 days. The LOCEAN expertise center of the Centre Aval de Traitement des Données SMOS has produced 18-day SSS maps over a 0.25 × 0.25° EASE grid over the 2010–2016 period (Boutin et al., 2017). These maps are available every 4 days. This product features a methodology for the removal of coastal and latitudinal SSS biases based on an update of Kolodziejczyk et al. (2016) and further described by Boutin et al. (2018).

SSS has also been retrieved from two National Aeronautics and Space Administration (NASA) satellite instruments from August 2011 to present. Aquarius/SAC-D is a collaborative effort between NASA and the Argentine Comisión Nacional de Actividades Espaciales. Aquarius' native spatial resolution is about 100 km, and global coverage is acquired over 7 days. The Aquarius Version 4.0, level 3 gridded SSS data set developed by the Aquarius Data Processing System over the satellite data record (25 August 2011 to 7 June 2015), is used in the present study. It is gridded to a 1° spatial resolution averaged over 7 days. The product is available from the Physical Oceanography Data Active Archive Centre.

The SMAP mission builds on the Aquarius/SAC-D legacy. Its native spatial resolution (40 km) is comparable to SMOS with an increased spatiotemporal coverage (revisit at least every 3 days). Remote Sensing System provides an 8-day running mean gridded SSS product on a 0.25° × 0.25°, daily grid from 1 April 2015 to present. Its version 2 is also available through the Physical Oceanography Data Active Archive Centre.

All salinity products are following the Practical Salinity Scale-1978 (Unesco et al., 1981) and are thus unitless.

To complement the SSS analysis presented in this study, several products based on remote sensing were used: SLA, surface currents, precipitation, and evaporation.

The Copernicus Marine and Environment Monitoring Service (CMEMS) has processed and distributed daily maps of SLA and geostrophic currents from 1993 to present using all satellite altimeter measurements available at a given time. Anomalies are referenced to the 1993–2002 period. This L4 product is available in its version 5.0 on a 0.25° × 0.25° grid. Based on SLA, an atlas of mesoscale eddy trajectories, produced by AVISO following the methodology of Chelton, Gaube, et al. (2011) and Chelton, Schlax, and Sameslon (2011), is available from 1993 to 2016. It is referred to as the Chelton-Schlax-Sameslon (CSS) Atlas hereafter.

The Global Precipitation Climatology Project provides monthly precipitation globally on a 2.5° × 2.5° grid with associated errors from 1979 to present (Adler et al., 2003). Version 2.3 is used in this paper. Global Precipitation Climatology Project uses satellite remote sensing together with rain gauges. Its full description is found in their technical report (see Acknowledgments).

The Objectively Analyzed Air-sea Fluxes project provides evaporation estimates on a monthly 1° × 1° spatial grid from 1958 to present in its version 3 (Yu et al., 2008). This product is based on a series of satellites combined with reanalysis outputs produced from NCEP and ECMWF models, based on in situ and numerical modeling.

To facilitate analysis of the various data products, all data sets are regridded to a 0.5 × 0.5° horizontal mesh every 4 days using linear interpolation to come close to the SMOS and SMAP native resolutions. They are then smoothed according to the SMOS data set used in the present study using an 18-day running average to limit high-frequency variability.

2.2. Zonal Wave Number-Frequency Spectra

Zonal wave number-frequency spectra were estimated from the different variables to examine the dominant temporal and spatial scales.

The spectra were computed following the methodology described in Farrar (2008) and Farrar and Weller (2006) using a two-dimensional fast Fourier transform. The data sets were first detrended in time, and the edges were tapered to zero over 10° in longitude and 150 days in time using a Tukey (cosine taper) window. Data gaps from islands such as Clipperton Island (10°N, 109°W) and from remaining RFI-filtered pixels were filled by linear interpolation in longitude. In order to limit the noise, spectra were computed over 3° of

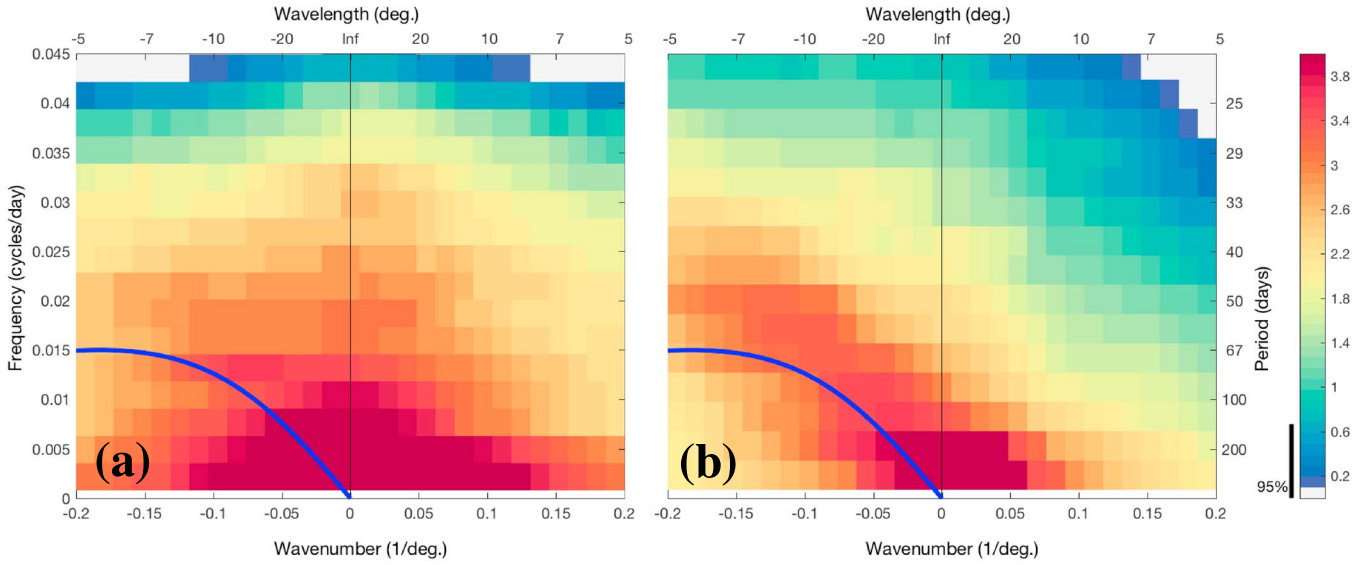

Figure 2. Log 10 of the zonal wave number-frequency power spectral density (colors) of (a) Soil Moisture and Ocean Salinity sea surface salinity (cpd^{-1} deg^{-1}) and (b) Copernicus Marine and Environment Monitoring Service sea level anomaly ($cm^2 \cdot cpd^{-1} \cdot deg^{-1}$) averaged over 9°–11°N computed over 2010–2016 and between 150° and 85°W. For reference, the free, first baroclinic mode Rossby wave dispersion relation is shown as computed with the deformation radius given at (10.5°N, 125.5°W) by Chelton et al. (1998) and a meridional wave number of zero (thick blue line). The 95% confidence interval is given by the black marker in the colorbar. Both fields reveal the presence of westward propagating features.

latitude and averaged, as their noise is assumed to be uncorrelated. The obtained spectra were further averaged over five adjacent frequency and wave number bands.

Cross-spectra are used in the assessment of the salinity budget. The cross-spectrum of two fields gives their coherence amplitude, coherence phase, and gain in the zonal wave number-frequency domain (Farrar, 2008). The coherence can be used to estimate the correlation as a function of frequency between the various terms of the salinity budget (e.g., SSS tendency and freshwater fluxes and horizontal advection). Cross-spectral analysis is also useful when comparing two identical variables measured from different platforms. Assuming the noise from SMOS, Aquarius, and SMAP are independent, the coherent variability should be close to reality. When performing cross-spectra, all data sets are linearly interpolated to the SMOS grid.

3. Results

3.1. SSS Variability Observed by Various Satellites

Visual inspection of monthly maps of SSS and currents suggests the imprint on the SSS fields of the eddies described in section 1 (Figure 1 and Movie S1). The three eddies identified on 1 March 2014 in the ETPac are associated with distinctive low SSS (Figure 1). When looking at the entire SMOS period along 10°N, we find significant westward-propagating energy in the SSS field centered at 70-day period and 15° zonal wavelength (Figure 2a). At timescales longer than 150 days, SSS variability is high with no significant propagation along 10°N (Figure 2a). This is associated with known biannual, seasonal, and longer timescale variability as described in section 1. The SMOS SSS power spectrum shows energy at nearly all frequency and wavelength bands.

Taking advantage of the satellite SSS data sets from three distinct platforms, we can evaluate their common signal. The cross-spectra at 10°N of Aquarius and SMAP SSS with SMOS SSS enable us to quantify the coherence of their signal during their common period. Assuming their noise to be independent, the noise coherence is negligible, and coherent physical features stand out. The cross-spectra of SMOS and Aquarius as well as that of SMOS and SMAP show good consistency (Figure 3). Westward propagation of SSS signal along 10°N at the Rossby wave speed is consistently detected by SMOS, Aquarius, and SMAP. The Aquarius-SMAP cross-spectrum was not computed because their common period of observation is too short. In the 7–15° zonal wave number and 50- to 100-day frequency area, SMOS and Aquarius have a common

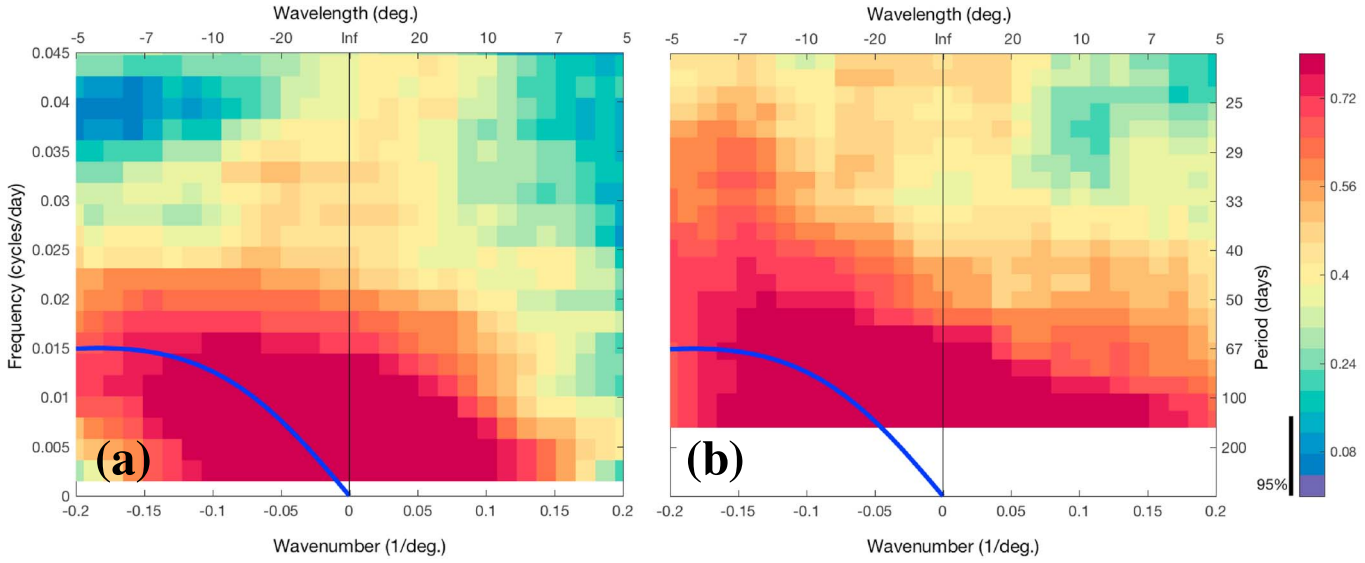

Figure 3. Zonal wave number-frequency coherence amplitude of Soil Moisture and Ocean Salinity (SMOS) sea surface salinity and (a) Aquarius and (b) Soil Moisture Active Passive (SMAP) sea surface salinity averaged over 9°–11°N computed over the common period with SMOS (2011–2015 for Aquarius and 2015–2016 for SMAP) and between 150° and 85°W. The 95% confidence interval is given by the black marker by the color bar. Aquarius and SMAP show coherent variability with SMOS at the intraseasonal timescale, 50–180 days.

variance of 70% and SMOS and SMAP of above 75%. The difference between the two sets of data sets is likely due to the increase of spatial resolution and of spatiotemporal sampling from Aquarius to SMOS and SMAP.

The consistency of SMOS SSS with other space-borne SSS products give us confidence in using the longer SMOS SSS record to study intraseasonal variations in the ETPac. Aquarius and SMAP are therefore not used in the subsequent spectra in this paper.

3.2. SSS and SLA Variability at 10°N

The zonal wave number-frequency spectrum of SLA shows significant energy along 10°N at the intraseasonal timescale with signal propagation at a speed similar to the propagation speed of long Rossby waves (Figure 2b). This is consistent with the signal found in SSS (Figure 2a). This SLA energy peak is associated with the eddies created near the southern North America and Central American Coasts and exported westward along 10°N (see section 1).

Motivated by the SSS and SLA spectra, a 50- to 150-day Butterworth filter was used to isolate the signal of interest. The propagation of the filtered SLA at 10°N extends from the easternmost ETPac (85°W) to about 135°W over the course of 6 to 9 months (Figure 4d). The SLA shows the longitudinal extent of the Tehuantepec and PE's journey. Filtered SSS from all satellite products show consistent propagation with analogous characteristics across most of the longitude range observed by SLA (Figure 4). The features are about 3° wide in longitude and travel at a speed of about 0.17 m/s. This is consistent with the propagation observed from the power spectra (Figures 2 and 3). Even though the SSS signal is noisier than SLA, it provides a complementary tool to study physical processes associated with this intraseasonal variability during the life of the eddies.

In the following, we investigate the physical processes causing the intraseasonal SSS variability observed along 10°N. The consistency of the intraseasonal SLA and SSS anomalies propagation speeds (Figure 4) highlights the impact of ocean dynamics. The SSS in this region is also affected by freshwater fluxes. In order to quantify the role of each process, the salinity budget based on observations was computed following Hasson et al. (2014). It is expressed in its simplified form as

$$\frac{\partial S}{\partial t} = \frac{(E-P)S}{H} - \vec{u}\cdot\vec{\nabla}S + res., \tag{1}$$

where S is the mixed layer salinity, t is time, H is the mixed layer depth, and $\vec{u}$ is the horizontal current. The term on the left-hand side of equation (1) will be referred to as SSS tendency, the first term on the right as

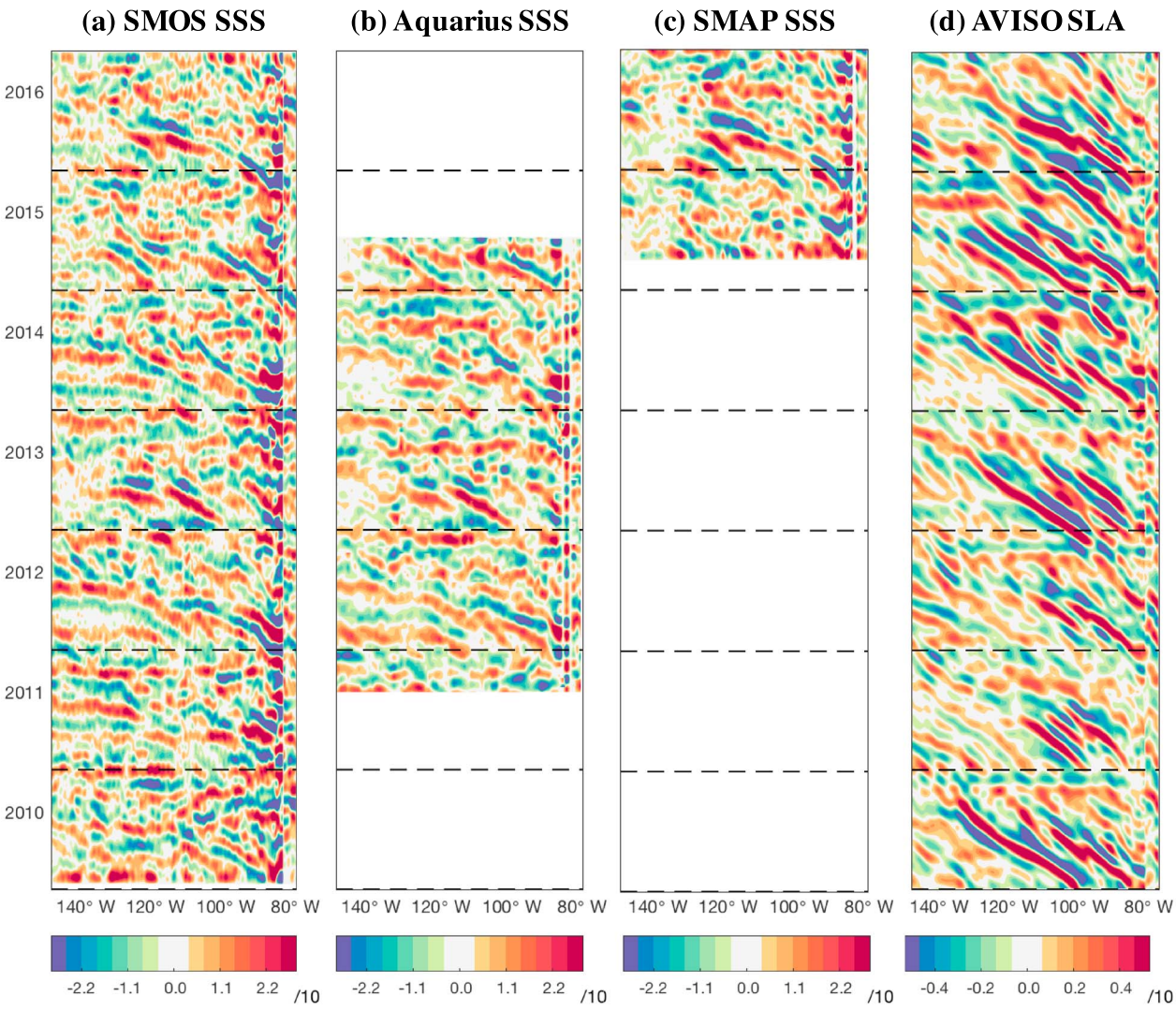

Figure 4. Longitude-time plot of sea surface salinity (SSS) anomalies filtered between 50 and 180 days averaged between 9° and 11°N from (a) Soil Moisture and Ocean Salinity (SMOS), (b) Aquarius, and (c) Soil Moisture Active Passive (SMAP). Equivalent anomalies are computed for (d) Copernicus Marine and Environment Monitoring Service sea level anomaly (SLA; cm). All SSS and SLA products show the features propagating from 80° to 135°W with a seasonal cycle in their intensity.

freshwater flux, and the second one as horizontal advection. The residual (*res.*) is comprised of vertical processes, horizontal subgrid-scale processes, and observational errors; none of which are individually quantifiable from observations in the present study.

Observations allow the estimation of SSS, E, P, and $\vec{u}$. Some assumptions were made to estimate the first three terms of equation (1). First, we assume that SSS represents the average mixed layer salinity. Although this assumption is inaccurate in rainy environments such as the ETPac, which has strong shallow stratification under low wind conditions, most of the fresh anomalies associated with heavy rains disappear from the SMOS SSS fields after a few hours (Supply et al., 2017). ETPac eddies are long lived, and it is assumed that on longer timescales the salinity in the mixed layer within the eddies is vertically well mixed. Moreover, the mixed layer depth is modulated by the eddy structure. Liang et al. (2012) found an averaged depth between 50 and 100 m from a numerical simulation for the ETPac eddies. H was fixed to 100 m in the present study.

Following equation (1), the SSS budget was estimated along 10°N and reveals the leading role of horizontal advection in the SSS intraseasonal variations. The cross-spectrum of the SSS tendency and the freshwater

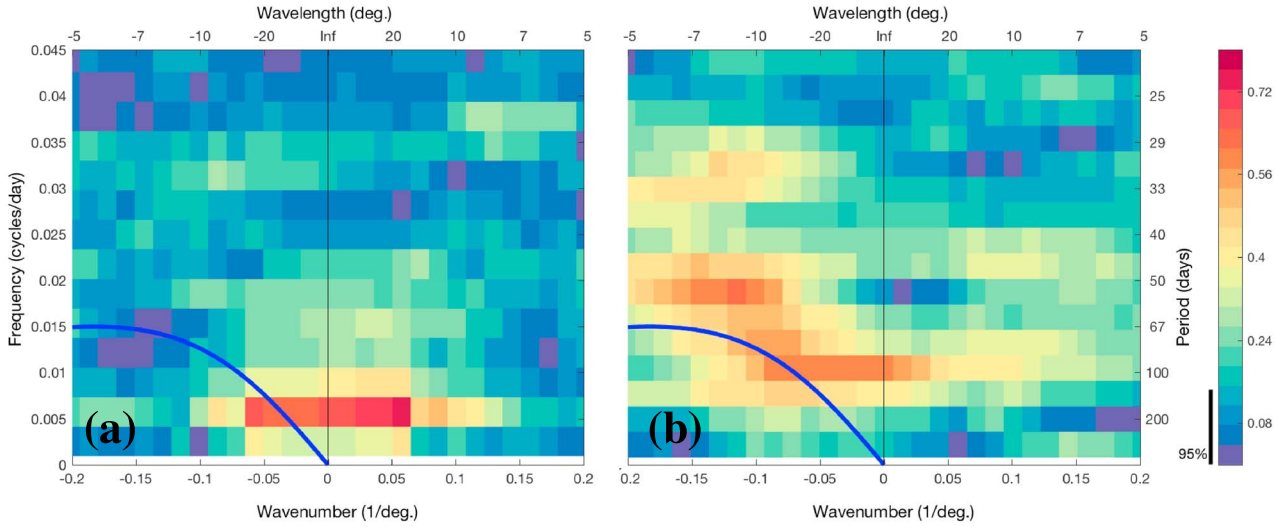

Figure 5. Zonal wave number-frequency coherence amplitude of Soil Moisture and Ocean Salinity sea surface salinity (SSS) tendency and (a) freshwater fluxes and (b) horizontal advection based on equation (1). Cross-spectra averaged over 9°–11°N and computed for the Soil Moisture and Ocean Salinity period (2010–2016) and between 150° and 85°W. The 95% confidence interval is given by the black marker by the color bar. Freshwater fluxes mainly explain nonpropagating SSS variability at the biannual timescale whereas the horizontal advection explains about 50% of the intraseasonal westward propagating signal in SSS.

fluxes is shown in Figure 5a. Those for the SSS tendency and the horizontal advection are shown in Figure 5b. The freshwater fluxes explain about 70% of the variance of SSS tendency at the semiannual frequency and at large zonal wavelength as expected by the biannual passage of the ITCZ at 10°N (Figure 5a). Forcing from the freshwater fluxes has little coherence with SSS tendency in the remaining frequency-wavelength domain. Over time, eddies indeed lose their SST signature and therefore, following Bulk formula, have limited direct impact on the freshwater fluxes. Horizontal advection explains above 50% (values above 0.5 on Figure 5b) of the SSS tendency variance in the negative 7–15° zonal wavelength and 50- to 150-day frequency band. This is consistent with eddies generated in the Gulfs of Tehuantepec and Papagayo being responsible for the variability observed along 10°N as suggested above.

The following sections aim at further describing the nature of these eddies and their SSS signal.

3.3. Transport of Anomalies

The long-lived ETPac eddies could have an impact on the extension of the ETPac freshpool by trapping and transporting freshwater to the west. Most eddies are formed near the ETPac freshpool where extremely low SSS waters are found and may carry in their core some trapped fluid from their formation site.

Mesoscale eddies from the CSS Atlas were selected using the following criteria (all must be reached at least once in each eddy's life): amplitude > 20 cm, radius > 100 km, and age > 30 days. Most eddies originate near the southern North America and Central American coasts and travel to the 10°N latitude and then westward (Figure 6). Eddies are classified in three categories depending on their origin. Over the 2010 to mid-2016 period, eight eddies were formed in the Gulf of Papagayo (Cat. 1), seven in the Gulf of Tehuantepec (Cat. 2), and four around 100°W and 12°N (Cat. 3). In 2014, one eddy of each category was captured by the CSS Atlas as shown on 1 March. One eddy associated with high SSS centered at (105°W, 12°N) is not selected by the chosen thresholds (Figure 1). Only one eddy was found to be cyclonic between 2010 and 2016. All eddies but three have a negative SSS anomaly (SSSA) signature. SSSA refers to a spatial anomaly, that is, the eddy core SSS minus the outside SSS. The eddy "core SSS" is a 1° box average around its center location given by the CSS Atlas. The "outside SSS" corresponds to an average of all points between 1.5° and 3° away from the eddy's center.

Cat. 1 Gulf of PE are formed between November and December and always go through the same location at [90°W, 11°N] just west of the Papagayo gap in the Cordillera (Figure 6a). Their centroids all follow a 2°-wide southwestward path and reach 100°W–10°N about 4 months later. One exception is an eddy formed in March 2016 that has a peculiar behavior traveling north with a positive SSSA and not passing through

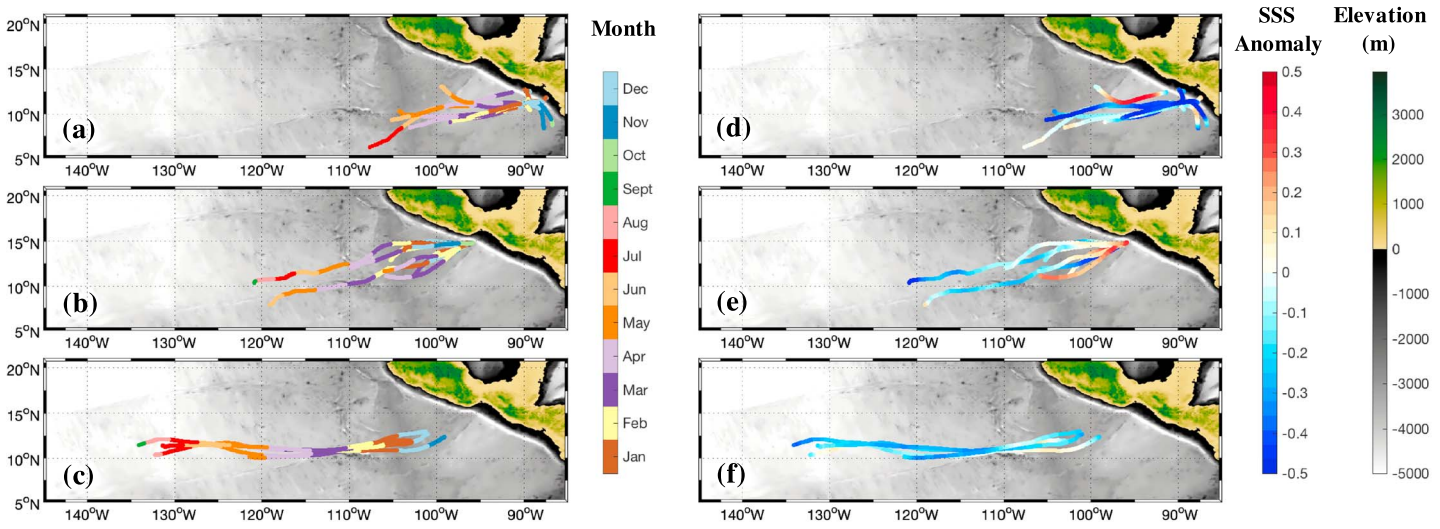

Figure 6. Eddy positions from the Chelton-Schlax-Sameslon Atlas. Colors represent (a–c) the month of the year and (d–f) the sea surface salinity (SSS) spatial anomaly relative to the surroundings corresponding to each position. The SSS spatial anomaly is a 1° × 1° average centered on the eddy center relative to surrounding SSS, between 1.5° and 3° from the eddy center. The eddies were sorted in three categories depending on the location where they were first tracked: Those formed in the Gulf of Papagayo (a and d), those formed in the Gulf of Tehuantepec (b and e), and those formed in the open ocean (c and f). Ocean depths and land elevations (in meters) are indicated by the second color scale in the right column. The consistent timing of the eddies of each category is remarkable. Most eddies show negative SSS anomalies throughout their lives.

[90°W, 11°N]. This eddy is cyclonic, while all the others are anticyclonic. Most PE have a negative SSSA signature (Figure 6d), four of them having anomalies reaching −0.5 most of their (tracked) lives.

Cat. 2 Tehuantepec Eddies (TE) depart the coastal area from (96°W, 15°N) between October and January (Figure 6b). They are all generated in a very localized area, just south of the Tehuantepec Canyon and travel southwest. TE have an average life of 5 months, but two eddies almost reach as far as 119°W in about 8 months. The SSSA signature of the TE is heterogeneous (Figure 6e). The two short-lived TE display a steady positive SSA (+.3), and the two long-lived ones a steady negative SSSA (−.3).

A third category of eddies is detected in the open ocean and hereafter referred to as open ocean eddies (OCE). Analogously to the PE and TE, the OCE are formed within a few degrees and within a few weeks of the year from each other; that is, around (100°W, 12°N) and in December (Figure 6c). The eddies are advected west of their formation site along 10°N with the presence of the seasonal NEC. The four eddies detected between 2010 and 2016 follow a narrow undulating pathway. One must keep in mind that the four eddies develop in different years. Three out of the four OCE travel westward past 130°W about 8 to 9 months after the tracking begins. The farthest-reaching OCE occurs during 2014 and is located at 110°W on 1 March 2014 (Figure 1). OCE have on average a negative SSSA signature (Figure 6f). All eddies pass just to the north of the volcano-studded ridge centered on (11°N, 101–107°W), near Clipperton Island, as revealed by the bathymetry (gray shading, Figure 6). This ridge is part of the Clipperton Fracture Zone extending from the Tehuantepec marine Ridge to the Line Islands (Menard & Fisher, 1958).

Eddies from all categories exist in an anticyclonic mean zonal shear at the seasonal timescale (Figure 7). From November to January, westward zonal currents are found near the American coast, just south of the formation region and the pathways of eddies from all categories (Figures 7a, 7d, and 7g). Moreover, this period also coincides with the peak Nortes wind season. In the subsequent period (February–April), both NEC and NECC strengthen and create a strong anticyclonic mean zonal shear zone. Most eddies from all categories follow this shear zone closely and especially the OCE ones (Figures 7b, 7e, and 7h). In the last 3-month period (May–July), mostly OCE (Cat. 3) remain, as they are formed later during the year and have the longest lives. Even though the NEC weakens, the OCE keep following the zonally oriented shear zone along about 12°N (Figure 7i).

Two eddies were found not to fit in these three categories and showed peculiar behavior. They were formed during June 2015 and June 2016. They were generated in the Gulf of Papagayo vicinity at an odd time of the

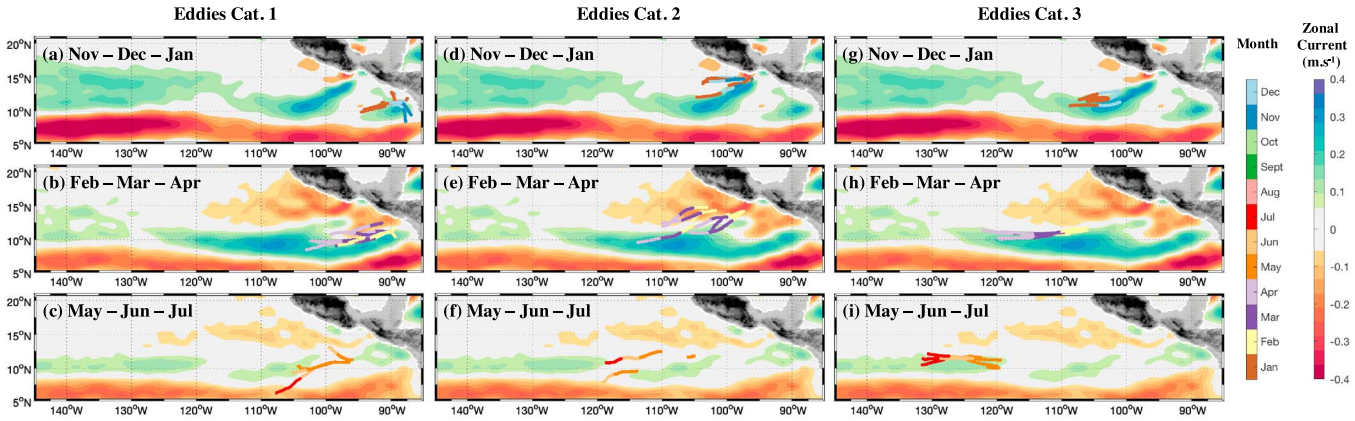

Figure 7. The 2010–2016 mean Copernicus Marine and Environment Monitoring Service zonal currents for November-December-January (a, d, and g), February-March-April (b, e, and h), and May-June-July (c, f, and i) for the three eddies categories (a–c, d–f, and g–i). As in Figure 6, overlaid colors represent the position and the month of the year of eddies from the Chelton-Schlax-Sameslon Atlas. Eddies from all categories exist in an anticyclonic mean zonal shear at the seasonal timescale.

year and followed roughly the OCE pathway after reaching the 10°N latitude. These peculiar occurrences might be linked to interannual variability. ETPac atmospheric and oceanic circulations were strongly altered by the occurrence of one of the strongest El Niño events on record from April 2015 to April 2016 (Blunden & Arndt, 2016). They will not be considered in the rest of this study.

Eddies transporting anomalously fresh (or, sometimes, salty) waters from the American coast along 10°N can impact the overall salinity budget of the region and might shape the extension of the ETPac freshpool described by Guimbard et al. (2017). Moreover, eddies have a strong seasonality (Figures 6a–6c) and could affect the seasonal variability in the ETPac freshpool. The advective nonlinearity parameter or "bolus transport" measures the capacity of an eddy to advect a parcel of trapped fluid within the eddy interior (Chelton, Gaube, et al., 2011; Chelton, Schlax, & Sameslon, 2011). It is defined as U/c, where U is the maximum rotational speed and c the translation speed of the eddy. U is readily provided by the CSS Atlas and c is computed from successive positions. When eddies have $U/c \geq 1$, it implies that there is trapped fluid that is advected within the eddy as it translates. OCE have U/c values well over 1 for about the first 3 months of their lives (Figure 8). PE also show high U/c values after passing [90°W, 11°N]. U/c drops below 1 around March each year. Only two TE have U/c over 1 (Figure 8b). PE and OCE trap low SSS waters and efficiently carry them from 90° to 100°W and from 100°W to 110°W, respectively.

Even though the values of U/c are only marginally above 1, the SSSA fields hint that the eddies may carry fresh water as far as 135°W (Figures 6d–6f). The advective nonlinearity parameter is almost surely underestimated: the maximum rotational speed (U) will be underestimated because of the smoothing involved in producing the gridded altimetry product used for estimating the rotational speeds. It is also possible that other processes help maintain the anomaly within the eddy core. All eddies have SSSA that show variations with time and sometimes change from positive to negative. SSSA is modified by exchanges of fresh water between the eddy's core and its surroundings but also by changes in the "outside SSS" as the eddy travels through steep SSS fronts.

In order to study the modifications of the eddies' core SSS without the dependence on the "outside SSS," SSS changes within their core and along their translation are investigated in the following section.

3.4. The Evolution of SSS Anomalies Within the Eddies

As the eddies travel westward between 10° and 15°N, the anomalous salinity that they transport is modified along their journey. All eddies show strong variability in their core SSS (Figure 9). In this section, the term "SSS deviation" (SSSD) is used to refer to the departure of an eddy's SSS value from the average SSS over the first 10 days it was detectible. Negative and positive deviations are seen along each eddy's journey ranging from −0.1 to +0.1. The SSSD amplitude (Figure 9) is a fifth of the SSSA variations (Figure 6), again reinforcing the notion that the eddies carry SSS anomalies over long distances. In order to investigate SSSD from the

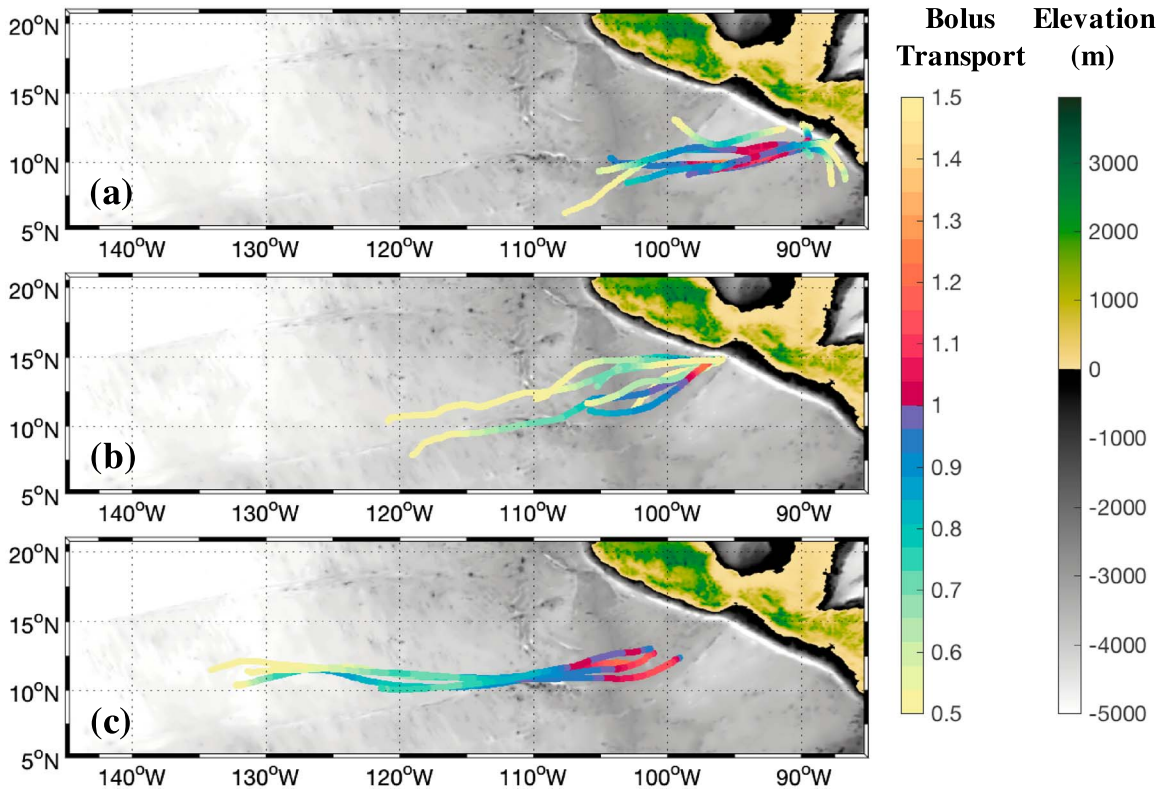

Figure 8. Bolus transport: fraction of median Eddy translation speed/maximum rotation velocity (U/c). Same categories (a–c) as for Figures 6a–6c. Eddies have U/c values over 1 for to up 4 months.

eddies' cores, we develop a budget from a "Lagrangian" moving frame of reference. The budget follows the location of the eddy with its translation speed. The advection term in equation (1) becomes null within the eddy core as particles rotate around the eddy center. The conservation equation can therefore be expressed as

$$\text{res.} = \frac{\partial S}{\partial t} - \frac{(E-P)S}{H}. \quad (2)$$

As stated above, the residual term includes processes that are not quantifiable from observations as well as observational errors. If it is assumed that observational errors are negligible (or at least constant in time), changes in the residual indicate variations in vertical advection as well as small-scale processes, that is, exchanges of the eddy core waters with surrounding waters.

Positive deviations (core SSS increasing with time) are expected to result from evaporation as well as mixing with the surrounding waters when the ambient water is saltier. Mixing depends on the inside/outside SSS gradient, that is, the SSSA. For instance, TE holding positive SSSA shows a negative SSSD here (Figures 6d and 9a). This is consistent with the fact that mixing in this case would decrease the eddy SSS. Negative deviations (core SSS decreasing with time) are expected to be due to rainfall in most cases. SSSA are mainly negative (Figures 6 d–6f). Note that PE SSSD abruptly change sign as they pass [90°W, 11°N] (Figure 9a), just as the advective nonlinearity parameter rises above one (Figure 8a).

The freshwater fluxes are positive for the first half of the eddies' lives and become negative afterward (Figures 9b, 9c, and 10a). The position of the trade winds and the ITCZ explains this pattern. From December to March, the ITCZ is close to the equator, and the strong and steady northeasterly trade winds are to its north. Low precipitation and strong evaporation from the winds lead to positive freshwater fluxes. In boreal spring the ITCZ shifts north following the sun and brings high precipitation and wind convergence leading to negative freshwater fluxes. Their impact on SSSD is considerable. Assuming that the surface fluxes mostly vary on a scale larger than that of the eddies, they should not have an impact on SSSA.

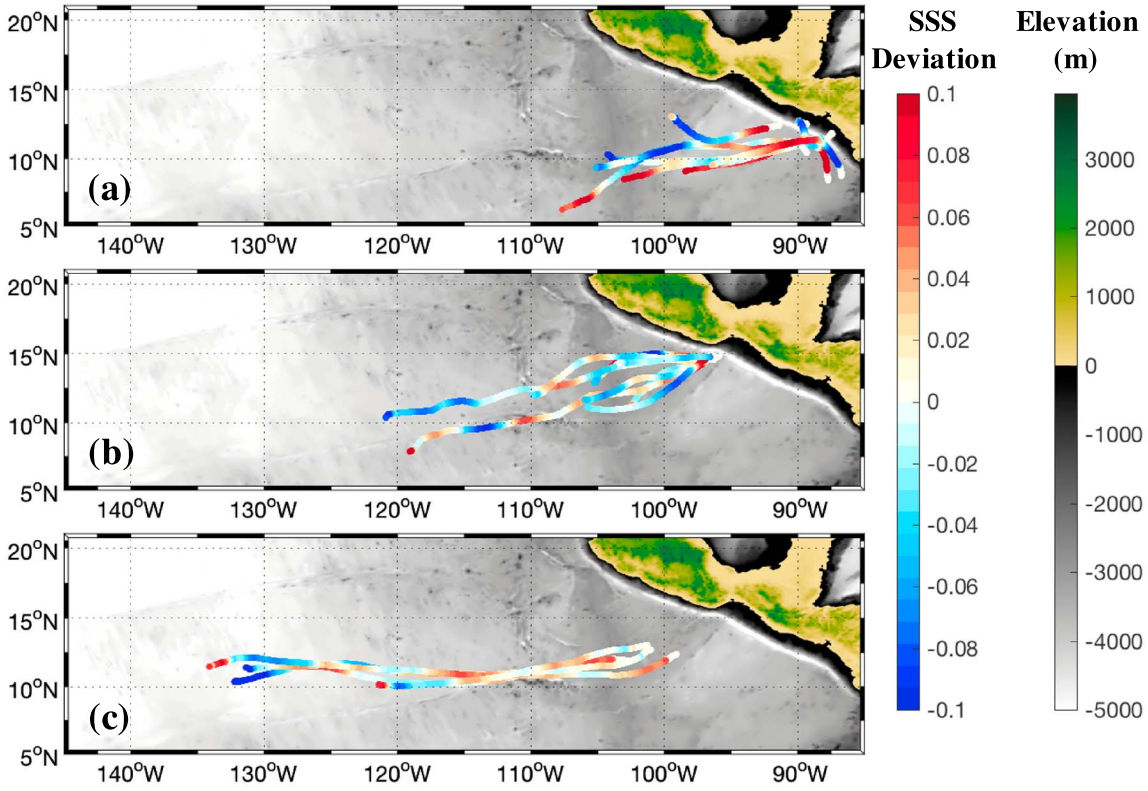

Figure 9. Eddies Sea surface salinity (SSS) deviation from the SSS at the time of formation (average of the 10 first days) within 1° of their trajectories from the Chelton-Schlax-Sameslon Atlas. Same categories (a–c) as for Figures 6a–6c. Small variations of SSS with time are found within the eddies.

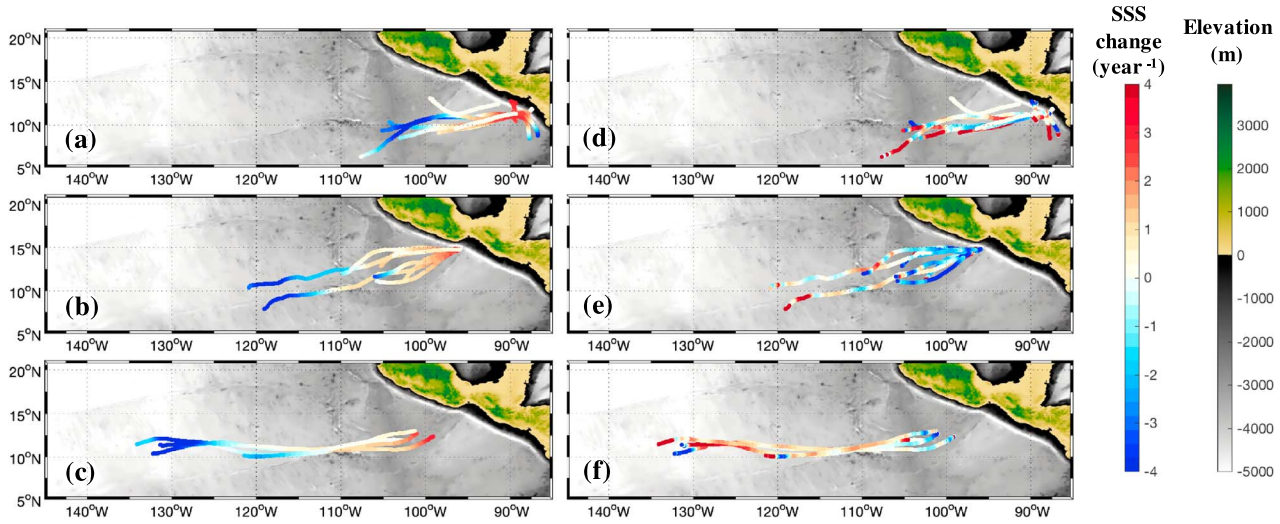

Figure 10. (a–c) Freshwater fluxes and (d–f) residual based on equation (2) within 1° of the eddies trajectories from the Chelton-Schlax-Sameslon Atlas (per year). Same categories as for Figure 6. Freshwater fluxes strongly force the eddies sea surface salinity (SSS) following the displacement of the Intertropical Convergence Zone. Changes in SSS are very strong at the end of most eddies' lives.

Mixing and vertical advection are more difficult to estimate and are hypothesized here to be described by the residual term of equation (2). The residual amplitude is of the same order of magnitude as the freshwater fluxes but shows smaller-scale variations (Figures 10d–10f). As described above, assuming the observational errors are limited, the residual is directly linked to exchanges with the surrounding waters and therefore to SSSA. In that case, positive SSSA leads to negative residuals, and vice versa. This is especially marked for OCE and positive SSSA TE throughout their lives. Mixing and vertical advection are modifying the PE before reaching the [90°W, 11°N] in a region of strong vertical stratification. Moreover, mixing decreases the SSSA, which materializes as a sharp increase of the residual amplitude (and decrease of SSSA) toward the end of the eddies' lives. This phenomenon is apparent for most eddies and especially for PE. PE have indeed the strongest SSSA signature, as they are formed directly within the ETPac freshpool and have rather short lives (about 5 months). SSS therefore reveals the PE abrupt end of life from mixing.

The similarity of the eddies' life cycles (i.e., when/where they are formed and when/where they dissipate based on SLA and the SSS signal) demonstrates the ability of SSS to give additional insight into their dynamics above SLA alone.

4. Discussion and Conclusions

This study of the SSS signal associated with eddies generated in the north ETPac has two implications. On the one hand, eddies trap and carry water in their core westward up to 40° of longitude away from the coast. SSS can be used to trace this water that holds critical nutrients in a region of relatively low production. On the other hand, SSS provides an unprecedented data set to study the eddies' dynamics. SSS can be used as an indicator for mixing of the core waters with its environment. Moreover, using the zonal wave number-frequency coherence amplitude of the multiple available satellite SSS data sets enabled us to highlight variability of interest (Figure 3).

The eddy-related SSS signal shows great consistency with SLA (Figure 4), attesting to the ability of SSS to trace the eddies. Moreover, the observed propagation of SSS and SLA anomalies from the power spectra are consistent with each other (Figures 2 and 3) as well as with previous descriptions of the TE and PE (Farrar & Weller, 2006). Other proxies such as SST and ocean color are greatly affected by air-sea fluxes and biological activity, respectively, and are not suited for tracking eddies over 4 months (Gonzalez-Silvera et al., 2004; Müller-Karger & Fuentes-Yaco, 2000). SSS on the other hand allows the study of eddies over most of their lives and therefore provides a tool to study the physical processes associated with their intraseasonal variability.

The SSS signal is also modified by freshwater fluxes; therefore, computing an SSS budget is needed to attempt to remove the freshwater flux signal and extract the signal associated solely with eddy dynamics.

Three categories of eddies were identified according to the location of first detection, and these showed consistent behavior from year to year, even though their number varies interannually. They also show strong seasonal variability. They were, respectively, formed in the Gulfs of TE and PE and in the open ocean at 100°W–12°N (OCE) between November and January and all traveled westward along 10°N. Nineteen eddies were studied over the SMOS period, 2010–2016, and only two were found to be cyclonic. SSS within the eddies is between −0.5 and +0.5 different from the surroundings. Some eddies were missed by the CSS Atlas and our thresholds as seen at [105°W, 12°N] on 1 March 2014 (Figure 1). This needs further investigation. Eddies from all categories are present in a zone of anticyclonic zonal mean shear. The reason behind the similarity of the PE behavior, all passing through [90°W, 11°N], some changing abruptly their salinity anomaly, still remains unsolved.

The OCE were of particular interest, as they have not been, so far as we know, described in the literature. They were found to be seeded near the coast and to grow substantially in the vicinity of the Clipperton Fracture Zone rise. Farrar and Weller (2006) described this region as being baroclinically unstable and therefore prone to growing instabilities. The presence of the OCE eddies in the zonal shear zone at the seasonal timescale and a visual evaluation of the currents and SSS evolution from monthly maps (not shown) supports the coastal-seeding-and-open-ocean-growing hypothesis.

The capacity of eddies to trap and carry fluid away from the formation zone is evaluated using the advective nonlinearity parameter comparing the eddy rotational and translational speeds (U/c, e.g., Chelton, Gaube,

et al., 2011; Chelton, Schlax, & Sameslon, 2011) derived from satellite altimetry. PE and OCE each appear to carry trapped waters at least 10° of longitude to the west. Further west, trapped fluid in the eddies' cores is modified by mixing with the surrounding waters. The amount of water brought to the west by eddies needs to be further evaluated in order to better understand their impact on the ETPac freshwater extension relative to other processes.

The modification of the SSS signal within the eddies' cores is further investigated. In a Lagrangian reference frame, the SSS is hypothesized to only be modified by freshwater fluxes and exchanges with water outside the eddies. SSS changes with time and freshwater fluxes are monitored by remote sensing, with the exchanges evaluated as a residual. Freshwater fluxes increase SSS outside of the ITCZ where evaporation is dominant and decrease SSS inside the ITCZ where precipitation is dominant. The eddies travel from outside the ITCZ to inside the ITCZ (which also moves meridionally during the year). The freshwater fluxes are removed from the SSS changes to isolate the effect of ocean dynamics. Ocean dynamics are most efficient when the SSS gradient across the eddies edge is strong but has a negative feedback, as it reduces this gradient. SSS reveals the importance of mixing and vertical processes at the end of the eddies' lives and highlights the prominence of mixing at their abrupt end (Figures 10d–10f).

These results are of particular interest for the Salinity Processes in the Upper Ocean Regional Study 2 (https://ourocean3.jpl.nasa.gov/spurs2/) experiment. The Salinity Processes in the Upper Ocean Regional Study 2 team has deployed extensive in situ assets from September 2016 to November 2017 in order to understand the small-scale processes at work behind the SSS variability in the ITCZ. Moorings were installed near (10°N, 125°W), which measured atmospheric fluxes as well as physical parameters within the water column. The imprint of the eddies discussed in this paper will be seen in their observations.

Acknowledgments
This research was carried out in part at the Jet Propulsion Laboratory (JPL), California Institute of Technology, under a contract with NASA and part at LOCEAN (Sorbonne Université, CNRS, IRD, MNHN) under a CNES Postdoctoral fellowship. This work is supported by NASA Grants NNX11AE83G and NNX14AH38G and is a contribution to the TOSCA/SMOS-Ocean proposal supported by CNES. We thank the reviewers for their thoughtfully comments that lead to a much-improved manuscript. We benefited from numerous data sets made freely available and are listed here: The SMOS debias_v2 SSS have been produced by LOCEAN laboratory and ACRI-st company that participate to the Ocean Salinity Expertise Center (CEC-OS) of Centre Aval de Traitement des Donnees SMOS (CATDS). of CATDS at IFREMER, Plouzane, France (http://www.catds.fr/Products, see documentation: http://www.catds.fr/Products/Available-products-from-CEC-OS/L3-Debiased-Locean-v2); the Aquarius/SAC-D and SMAP data was produced by Remote Sensing Systems and distributed by PODAAC (https://podaac.jpl.nasa.gov/dataset/AQUARIUS_L3_SSS_SMI_7DAY_V4; https://podaac.jpl.nasa.gov/dataset/SMAP_RSS_L3_SSS_SMI_8DAY-RUNNINGMEAN_V2); the SLA product is processed and distributed by CMEMS (http://marine.copernicus.eu); the global atlas of eddies is produced by AVISO (https://www.aviso.altimetry.fr/en/data/products/value-added-products/global-mesoscale-eddy-trajectory-product.html); the GPCP precipitation data set (http://eagle1.umd.edu/GPCP_CDR/Monthly_Data) is described in the project technical report (http://eagle1.umd.edu/GPCP_ICDR/GPCPmonthlyV2.3.pdf); Woods Hole Oceanographic Institution OAFlux evaporation data set (ftp://ftp.whoi.edu/pub/science/oaflux/data_v3); UCAR high-resolution terrain data set (High res terrain data set https://rda.ucar.edu/datasets/ds759.2/#!description); Chelton et al. (1998) Global Atlas of the First-Baroclinic Rossby Radius of Deformation and Gravity-Wave Phase Speed (http://www-po.coas.oregonstate.edu/research/po/research/rossby_radius/).

References

Adams, D. K., & Flierl, G. R. (2010). Modeled interactions of mesoscale eddies with the East Pacific Rise: Implications for larval dispersal. *Deep Sea Research Part I: Oceanographic Research Papers*, *57*(10), 1163–1176. https://doi.org/10.1016/j.dsr.2010.06.009

Adler, R. F., Huffman, G. J., Chang, A., Ferraro, R., Xie, P. P., Janowiak, J., et al. (2003). The version-2 global precipitation climatology project (GPCP) monthly precipitation analysis (1979-present). *Journal of Hydrometeorology*, *4*(6), 1147–1167. https://doi.org/10.1175/1525-7541(2003)004<1147:TVGPCP>2.0.CO;2

Alory, G., Maes, C., Delcroix, T., Reul, N., & Illig, S. (2012). Seasonal dynamics of sea surface salinity off Panama: The far Eastern Pacific Fresh Pool. *Journal of Geophysical Research*, *117*, C04028. https://doi.org/10.1029/2011JC007802

Barton, E. D., Lavín, M. F., & Trasviña, A. (2009). Coastal circulation and hydrography in the Gulf of Tehuantepec, Mexico, during winter. *Continental Shelf Research*, *29*(2), 485–500. https://doi.org/10.1016/j.csr.2008.12.003

Bingham, F. M., & Lee, T. (2017). Space and time scales of sea surface salinity and freshwater forcing variability in the global ocean (60°S-60°N): SPACE AND TIME SCALES OF SSSS. *Journal of Geophysical Research: Oceans*, *122*, 2909–2922. https://doi.org/10.1002/2016JC012216

Blunden, J., & Arndt, D. S. (2016). State of the climate in 2015. *Bulletin of the American Meteorological Society*, *97*(8), Si–S275. https://doi.org/10.1175/2016BAMSStateoftheClimate.1

Boutin, J., Vergely, J.-L., & Marchand, S. (2017). *SMOS SSS L3 debias v2 maps generated by CATDS CEC LOCEAN*. Issy-les-Moulineaux, France: SEANOE. https://doi.org/10.17882/52804

Boutin, J., Vergely, J.-L., Marchand, S., D'Amico, F., Hasson, A., Kolodziejczyk, N., et al. (2018). New SMOS Sea Surface Salinity with reduced systematic errors and improved variability. *Remote Sensing of Environment*, *214*, 115–134. https://doi.org/10.1016/j.rse.2018.05.022

Brown, C., Boutin, J., & Merlivat, L. (2015). New insights into fCO_2 variability in the tropical eastern Pacific Ocean using SMOS SSS. *Biogeosciences*, *12*(23), 7315–7329. https://doi.org/10.5194/bg-12-7315-2015

Chang, C. H., Xie, S. P., Schneider, N., Qiu, B., Small, J., Zhuang, W., et al. (2012). East Pacific ocean eddies and their relationship to subseasonal variability in central American wind jets. *Journal of Geophysical Research*, *117*, C10001. https://doi.org/10.1029/2011JC007315

Chelton, D. B., Schlax, M. G., & Samelson, R. M. (2011). Global observations of nonlinear mesoscale eddies. *Progress in Oceanography*, *91*(2), 167–216. https://doi.org/10.1016/j.pocean.2011.01.002

Chelton, D. B., deSzoeke, R. A., Schlax, M. G., El Naggar, K., & Siwertz, N. (1998). Geographical variability of the first baroclinic Rossby radius of deformation. *Journal of Physical Oceanography*, *28*(3), 433–460. https://doi.org/10.1175/1520-0485(1998)028<0433:GVOTFB>2.0.CO;2

Chelton, D. B., Freilich, M. H., & Esbensen, S. K. (2000). Satellite observations of the wind jets off the Pacific Coast of Central America. Part II: Regional relationships and dynamical considerations. *Monthly Weather Review*, *128*(7), 2019–2043. https://doi.org/10.1175/1520-0493(2000)128<2019:SOOTWJ>2.0.CO;2

Chelton, D. B., Gaube, P., Schlax, M. G., Early, J. J., & Samelson, R. M. (2011). The influence of nonlinear mesoscale eddies on near-surface oceanic chlorophyll. *Science*, *334*(6054), 328–332. https://doi.org/10.1126/science.1208897

Dong, C., McWilliams, J. C., Liu, Y., & Chen, D. (2014). Global heat and salt transports by eddy movement. *Nature Communications*, *5*, ncomms4294. https://doi.org/10.1038/ncomms4294

Farrar, J. T. (2008). Observations of the dispersion characteristics and meridional sea level structure of equatorial waves in the Pacific Ocean. *Journal of Physical Oceanography*, *38*(8), 1669–1689. https://doi.org/10.1175/2007JPO3890.1

Farrar, J. T., & Weller, R. A. (2006). Intraseasonal variability near 10 N in the eastern tropical Pacific Ocean. *Journal of Geophysical Research*, *111*, C05015. https://doi.org/10.1029/2005JC002989

Fournier, S., Vandemark, D., Gaultier, L., Lee, T., Jonsson, B., & Gierach, M. M. (2017). Interannual variation in offshore advection of Amazon-Orinoco plume waters: Observations, forcing mechanisms, and impacts: AMAZON-ORINOCO PLUME ADVECTION. *Journal of Geophysical Research: Oceans.*, *122*, 8966–8982. https://doi.org/10.1002/2017JC013103

Fournier, S., Vialard, J., Lengaigne, M., Lee, T., Gierach, M. M., & Chaitanya, A. V. S. (2017). Modulation of the Ganges-Brahmaputra river plume by the Indian Ocean Dipole and eddies inferred from satellite observations: Bay Of Bengal "river in the sea". *Journal of Geophysical Research: Oceans.*, *122*, 9591–9604. https://doi.org/10.1002/2017JC013333

Giese, B. S., Carton, J. A., & Holl, L. J. (1994). Sea level variability in the eastern tropical Pacific as observed by TOPEX and Tropical Ocean-Global Atmosphere Tropical Atmosphere-Ocean Experiment. *Journal of Geophysical Research*, *99*(C12), 24739. https://doi.org/10.1029/94JC01814

Gonzalez-Silvera, A., Santamaria-del-Angel, E., Millán-Nuñez, R., & Manzo-Monroy, H. (2004). Satellite observations of mesoscale eddies in the Gulfs of Tehuantepec and Papagayo (Eastern Tropical Pacific). *Deep Sea Research Part II: Topical Studies in Oceanography*, *51*(6–9), 587–600. https://doi.org/10.1016/j.dsr2.2004.05.019

Guimbard, S., Reul, N., Chapron, B., Umbert, M., & Maes, C. (2017). Seasonal and interannual variability of the Eastern Tropical Pacific Fresh Pool. *Journal of Geophysical Research: Oceans*, *122*, 1749–1771. https://doi.org/10.1002/2016JC012130

Hansen, D. V., & Maul, G. A. (1991). Anticyclonic current rings in the eastern tropical Pacific Ocean. *Journal of Geophysical Research*, *96*(C4), 6965. https://doi.org/10.1029/91JC00096

Hasson, A., Delcroix, T., Boutin, J., Dussin, R., & Ballabrera-Poy, J. (2014). Analyzing the 2010–2011 La Niña signature in the tropical Pacific sea surface salinity using in situ data, SMOS observations, and a numerical simulation. *Journal of Geophysical Research: Oceans*, *119*, 3855–3867. https://doi.org/10.1002/2013JC009388

Hasson, A., Puy, M., Boutin, J., Guilyardi, E., & Morrow, R. (2018). Northward pathway across the tropical north Pacific Ocean revealed by surface salinity: How do El Niño anomalies reach Hawaii? *Journal of Geophysical Research: Oceans*, *123*, 2697–2715. https://doi.org/10.1002/2017JC013423

Hasson, A. E. A., Delcroix, T., & Dussin, R. (2013). An assessment of the mixed layer salinity budget in the tropical Pacific Ocean. Observations and modelling (1990–2009) *Ocean Dynamics*, *63*(2–3), 179–194. https://doi.org/10.1007/s10236-013-0596-2

Kerr, Y. H., Waldteufel, P., Wigneron, J.-P., Delwart, S., Cabot, F., Boutin, J., et al. (2010). The SMOS mission: New tool for monitoring key elements of the global water cycle. *Proceedings of the IEEE*, *98*(5), 666–687. https://doi.org/10.1109/JPROC.2010.2043032

Kessler, W. S. (2006). The circulation of the eastern tropical Pacific: A review. *Progress in Oceanography*, *69*(2–4), 181–217. https://doi.org/10.1016/j.pocean.2006.03.009

Kolodziejczyk, N., Boutin, J., Vergely, J.-L., Marchand, S., Martin, N., & Reverdin, G. (2016). Mitigation of systematic errors in SMOS sea surface salinity. *Remote Sensing of Environment*, *180*, 164–177. https://doi.org/10.1016/j.rse.2016.02.061

Lagerloef, G., Colomb, F. R., Le Vine, D., Wentz, F., Yueh, S., Ruf, C., et al. (2008). The AQUARIUS/SAC-D Mission: Designed to meet the salinity remote-sensing challenge. *Oceanography*, *21*(1), 68–81. https://doi.org/10.5670/oceanog.2008.68

Lee, T., Lagerloef, G., Gierach, M. M., Kao, H.-Y., Yueh, S., & Dohan, K. (2012). Aquarius reveals salinity structure of tropical instability waves. *Geophysical Research Letters*, *39*, L12610. https://doi.org/10.1029/2012GL052232

Liang, J. H., McWilliams, J. C., Kurian, J., Colas, F., Wang, P., & Uchiyama, Y. (2012). Mesoscale variability in the northeastern tropical Pacific: Forcing mechanisms and eddy properties. *Journal of Geophysical Research*, *117*, L12610. https://doi.org/10.1029/2012JC008008

Melnichenko, O., Amores, A., Maximenko, N., Hacker, P., & Potemra, J. (2017). Signature of mesoscale eddies in satellite sea surface salinity data: SSS SIGNATURE OF MESOSCALE EDDIES. *Journal of Geophysical Research: Oceans*, *122*, 1416–1424. https://doi.org/10.1002/2016JC012420

Menard, H. W., & Fisher, R. L. (1958). Clipperton fracture zone in the northeastern equatorial Pacific. *The Journal of Geology*, *66*(3), 239–253. https://doi.org/10.1086/626502

Müller-Karger, F. E., & Fuentes-Yaco, C. (2000). Characteristics of wind-generated rings in the eastern tropical Pacific Ocean. *Journal of Geophysical Research*, *105*(C1), 1271–1284. https://doi.org/10.1029/1999JC900257

Palacios, D. M., & Bograd, S. J. (2005). A census of Tehuantepec and Papagayo eddies in the northeastern tropical Pacific. *Geophysical Research Letters*, *32*, L23606. https://doi.org/10.1029/2005GL024324

Périgaud, C. (1990). Sea level oscillations observed with Geosat along the two shear fronts of the Pacific North Equatorial Countercurrent. *Journal of Geophysical Research*, *95*(C5), 7239–7248. https://doi.org/10.1029/JC095iC05p07239

Piepmeier, J. R., Focardi, P., Horgan, K. A., Knuble, J., Ehsan, N., Lucey, J., et al. (2017). SMAP L-band microwave radiometer: Instrument design and first year on orbit. *IEEE Transactions on Geoscience and Remote Sensing*, *55*(4), 1954–1966. https://doi.org/10.1109/TGRS.2016.2631978

Samuelsen, A., & O'Brien, J. J. (2008). Wind-induced cross-shelf flux of water masses and organic matter at the Gulf of Tehuantepec. *Deep Sea Research Part I: Oceanographic Research Papers*, *55*(3), 221–246. https://doi.org/10.1016/j.dsr.2007.11.007

Stumpf, H. G., & Legeckis, R. V. (1977). Satellite observations of mesoscale eddy dynamics in the Eastern Tropical Pacific Ocean. *Journal of Physical Oceanography*, *7*(5), 648–658. https://doi.org/10.1175/1520-0485(1977)007<0648:SOOMED>2.0.CO;2

Supply, A., Boutin, J., Vergely, J.-L., Martin, N., Hasson, A., Reverdin, G., et al. (2017). Precipitation estimates from SMOS sea-surface salinity: Precipitation estimates from SMOS sea-surface salinity. *Quarterly Journal of the Royal Meteorological Society*, *144*, 103–119. https://doi.org/10.1002/qj.3110

Unesco, européennes, C. interuniversitaire d'études, Research, I. C. of S. U. S. C. on O., Ocean, I. A. for the P. S), (Joint Panel on Oceanographic Tables and Standards (1981). Background papers and supporting data on the International equation of state of seawater 1980. Unesco. Retrieved from http://books.google.fr/books?id=j3pNAQAAIAAJ

Willett, C. S., Leben, R. R., & Lavin, M. F. (2006). Eddies and tropical instability waves in the eastern tropical Pacific: A review. *Progress in Oceanography*, *69*(2–4), 218–238. https://doi.org/10.1016/j.pocean.2006.03.010

Yin, X., Boutin, J., Reverdin, G., Lee, T., Arnault, S., & Martin, N. (2014). SMOS sea surface salinity signals of tropical instability waves. *Journal of Geophysical Research: Oceans*, *119*, 7811–7826. https://doi.org/10.1002/2014JC009960

Yu, L., Jin, X., & Weller, R. A. (2008). Multidecade global flux datasets from the Objectively Analyzed Air-sea Fluxes (OAFlux) Project: Latent and sensible heat fluxes, ocean evaporation, and related surface meteorological variables. (OAFlux Project Technical Report) (P. 64pp.). Woods Hole Massachusetts: Woods Hole Oceanographic Institution.

Yu, L. (2015). Sea-surface salinity fronts and associated salinity-minimum zones in the tropical ocean. *Journal of Geophysical Research: Oceans*, *120*, 4205–4225. https://doi.org/10.1002/2015JC010790

Zhang, Z., Wang, W., & Qiu, B. (2014). Oceanic mass transport by mesoscale eddies. *Science*, *345*(6194), 322–324. https://doi.org/10.1126/science.1252418